Journal of Molecular Graphics and Modelling 38 (2012) 369–374

Contents lists available at SciVerse ScienceDirect

Journal of Molecular Graphics and Modelling

journal homepage: www.elsevier.com/locate/JMGM

Comparative electronic structures and UV–vis spectra of tribenzosubporphyrin, tribenzomonoazasubporphyrin, tribenzodiazasubporphyrin, and subphthalocyanine: Insight from DFT and TDDFT calculations

Yunling Gao[a,b], Pavlo V. Solntsev[a], Victor N. Nemykin[a,*]

[a] Department of Chemistry and Biochemistry, University of Minnesota-Duluth, Duluth, MN 55812, United States
[b] State Key Laboratory Breeding Base of Green Chemistry Synthesis Technology, College of Chemical Engineering & Materials Science, Zhejiang University of Technology, Hangzhou 310032, China

ARTICLE INFO

Article history:
Accepted 15 September 2012
Available online 25 September 2012

Keywords:
Subphthalocyanine
Subporphyrin
TDDFT
Electronic structure
Vertical excitation energies

ABSTRACT

Electronic structures, geometries, and vertical excitation energies of chloroboron subphthalocyanine, tribenzodiazasubporphyrin, tribenzomonoazasubporphyrin, and tribenzosubporphyrin were calculated using density functional theory (DFT) and time-dependent (TD) DFT coupled with polarized continuum model (PCM) approach. Molecular geometries calculated at the BP86/6-311G(d) level reveal bowl-shape, trigonal prismatic conformations for all compounds with a variable bowl-depth that depends on the number of *meso*-nitrogen atoms in corresponding molecule. TDDFT-PCM calculations predict that the Q-band should undergo gradual high-energy shift, while the B-band should undergo low-energy shift upon stepwise substitution of the *meso*-nitrogen atoms in subphthalocyanine toward tribenzosubporphyrin. The TDDFT-PCM predicted trend was rationalized on the basis of electronic structures of target macrocycles. When comparison between theory and experiment is available, TDDFT-PCM calculations are in qualitative and quantitative agreement with experimental data.

Published by Elsevier Inc.

1. Introduction

Phthalocyanines are well-explored aromatic macrocyclic compounds, which find various applications in industry and fundamental research [1]. The smallest phthalocyanine analogue is the subphthalocyanine macrocycle, which consists of only three isoindole fragments and three *meso*-nitrogen atoms [2]. Although subphthalocyanine was reported by Meller and Ossko in 1972 [3], its chemistry, redox and photophysical properties of its substituted analogues were only scarcely explored until 1990s [4–13], when several research groups became interested in their unique characteristics. Subphthalocyanines have nonplanar, bowl-like structures along with a 14 π-electron aromatic core with a trigonal-pyramidal boron atom as the central atom. They exhibit strong UV–vis absorption, intense fluorescence, and remarkable nonlinear optical properties and hence can be potentially applied as chromophores in molecular electronics [14–18], nonlinear optics materials [5,10–13,19–22], photodynamic therapy [23,24], and light-harvesting [25–29]. In 2006, the analogues of subphthalocyanines in which all *meso*-nitrogen atoms were substituted with the sp^2-hybrid carbons, the tribenzosubporphyrines [30], were synthesized and characterized as their boron complexes. Later, the *meso*-phenyl tribenzosubporphyrins were also reported by Luk'yanets, Kobayashi and co-workers [31]. Tribenzosubporphyrins also exhibit intense fluorescence, strong UV–vis absorption, and the similar to subphthalocyanine bowl-shaped geometry. In tribenzosubporphyrins, the Q-band is shifted to higher-energy and the B(Soret)-band is shifted to lower-energy compared to the subphthalocyanine [30].

To the best of our knowledge, however, no reports were published on the preparation and characterization of the subphthalocyanine analogues with one or two *meso*-nitrogen atoms substituted with sp^2-hybrid carbon atoms. In order to investigate the effect of stepwise substitution of *meso*-nitrogen atoms in subphthalocyanine with *meso*-carbon atoms on electronic structure and vertical excitation energies, we studied the full range of possible (aza)tribenzosubporphyrins (Fig. 1) using density functional theory (DFT) and time-dependent (TD) DFT coupled with polarized continuum model (PCM) approach. The data presented below highlight systematic changes of the electronic structure and spectroscopy in triisoindole-based aromatic macrocycles.

2. Experimental

The subphthalocyanine **1** was prepared and purified using published procedure [3], while a sample of

* Corresponding author.
E-mail address: vnemykin@d.umn.edu (V.N. Nemykin).

1093-3263/$ – see front matter. Published by Elsevier Inc.
http://dx.doi.org/10.1016/j.jmgm.2012.09.003

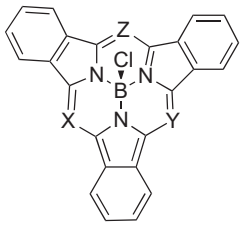

1	X=Y=Z=N
2H	X=CH,Y=Z=N
3H	X=Y=CH,Z=N
4H	X=Y=Z=CH
2Ph	X=CPh,Y=Z=N
3Ph	X=Y=CPh,Z=N
4Ph	X=Y=Z=CPh

Fig. 1. Target chloro subphthalocyanine derivatives.

meso-triphenyltribenzosubporphyrin was obtained from Prof. Luk'yanets group. The UV–vis spectra were recorded on Jascso V-670 spectrometer in dichloromethane as the solvent.

2.1. Computational methods

All DFT calculations were carried out using Gaussian 09 [32] software package running under UNIX OS. The molecular geometries were optimized in dichloromethane solvent using polarized continuum model (PCM) [33]. Combination of Becke's pure exchange functional [34] and Perdew's correlation functional [35] (BP86) coupled with 6-311G(d) basis set for all atoms was used in all calculations. Frequency calculations were performed on all optimized geometries to ensure that the obtained structures represent local minima. TDDFT-PCM calculations were conducted with BP86 functional coupled with 6-311G(d) basis set [36] and dichloromethane as a solvent media. GGA BP86 exchange-correlation functional was used in TDDFT-PCM calculations because, as it was shown before, it provides a better accuracy for energies of π–π^* transitions in porphyrinoids compared to more popular hybrid B3LYP exchange-correlation functional [37–39]. The first 50 excited states were calculated using equilibrium and non-equilibrium PCM solvation methods. Molecular orbital composition analysis was performed using QmForge program [40].

3. Results and discussion

Selected geometric parameters for DFT-PCM optimized molecular geometries of compounds **1**–**4** (Fig. 1) are listed in Table 1 and compared to those experimentally observed in subphthalocyanines and tribenzosubporphyrins. When comparison is possible, the optimized geometries are in good agreement with experimental structures. In all cases, the structures of studied molecules adopt the bowl-type conformation. The depth of the bowl in each specific compound depends on the number of *meso*-nitrogen atoms present in the structure (Table 1). Specifically, bowl depth monotonically decreases with the stepwise substitution of the *meso*-nitrogen by sp^2-hybridized carbon atoms with the subphthalocyanine structure having the largest and tribenzosubporphyrin having the smallest deviation from planarity. The optimized average C—N_{meso} and N—B bond distances are nearly the same among the compounds studied. DFT-predicted slightly shorter B—N bond distances in **4H** and **4Ph** compared to those experimentally observed in **4H-OMe**, **4H-OH**, and **4PhO-SiPh$_3$** (Table 1) can be attributed to the differences in axial ligands. Indeed, **4H** and **4Ph** have chlorine atom as an axial ligand, while **4H-OMe**, **4H-OH**, and **4Ph-OSiPh$_3$** have alkoxy- or hydroxy-groups as axial ligands. Finally, DFT-predicted B—Cl bond lengths monotonically increase with decreasing number of *meso*-nitrogen atoms.

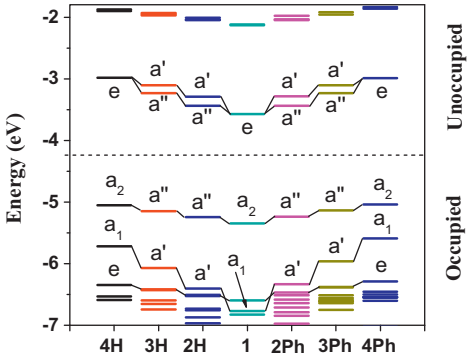

Fig. 2. Partial molecular orbital diagram for compounds **1**–**4** calculated at BP86/6-311G(d) level in DCM.

Molecular orbital energy diagrams for seven target molecules are presented in Fig. 2 and the analysis of their orbital compositions is presented in Fig. 3 and Tables S1–S7. The frontier orbitals for compounds **1**–**4** are also shown in the Supporting Information (Figs. S1–S7). In agreement with the previous data for compound **1** [41–44], it adopts C_{3v} symmetry with the LUMO and LUMO+1 being doubly degenerate and delocalized over the entire π-system. The HOMO is a non-degenerate a_2 symmetry MO, which has negligible electron density on nitrogen atoms. This orbital follows a pair of degenerate e symmetry MOs with significant contribution from the axial chlorine p_x and p_y AOs. Finally, the HOMO−3 has a significant contribution from the *meso*- as well as isoindole nitrogen atoms. Introduction of one C—H or C—Ph fragment in *meso*-position of the

Table 1
Comparison of the bond distances and the depths of bowl for all studied compounds.

	Bond distance (Å)				Depth of bowl (Å)[c]
	B—N[a]	C—N_{meso}[a,b]	B—Cl	C—C_{meso}[a,b]	
TDDFT-PCM					
1	1.489	1.348	1.906	–	2.59
2H	1.488	1.348	1.921	1.415	2.38
3H	1.488	1.348	1.939	1.413	2.19
4H	1.486	–	1.965	1.413	1.99
2Ph	1.486	1.348	1.923	1.426	2.32
3Ph	1.483	1.348	1.945	1.424	2.04
4Ph	1.480	–	1.975	1.423	1.74
Experimental (X-ray)					
1[d]	1.467	1.344	1.863	–	2.46
4H-OMe[d]	1.500	–	1.446[e]	1.406	1.66
4H-OH[d]	1.509	–	1.446[e]	1.399	2.35
4Ph-OSiPh$_3$[d]	1.501	–	1.414[e]	1.411	1.77

[a] Average bond distance.
[b] The carbon atom is the α-carbon of pyrrole ring.
[c] The bowl depth is defined as the distance from the boron atom to the mean plane of three lowest carbon atoms of the macrocycle.
[d] The crystal data.
[e] The bond distance of the B—O.

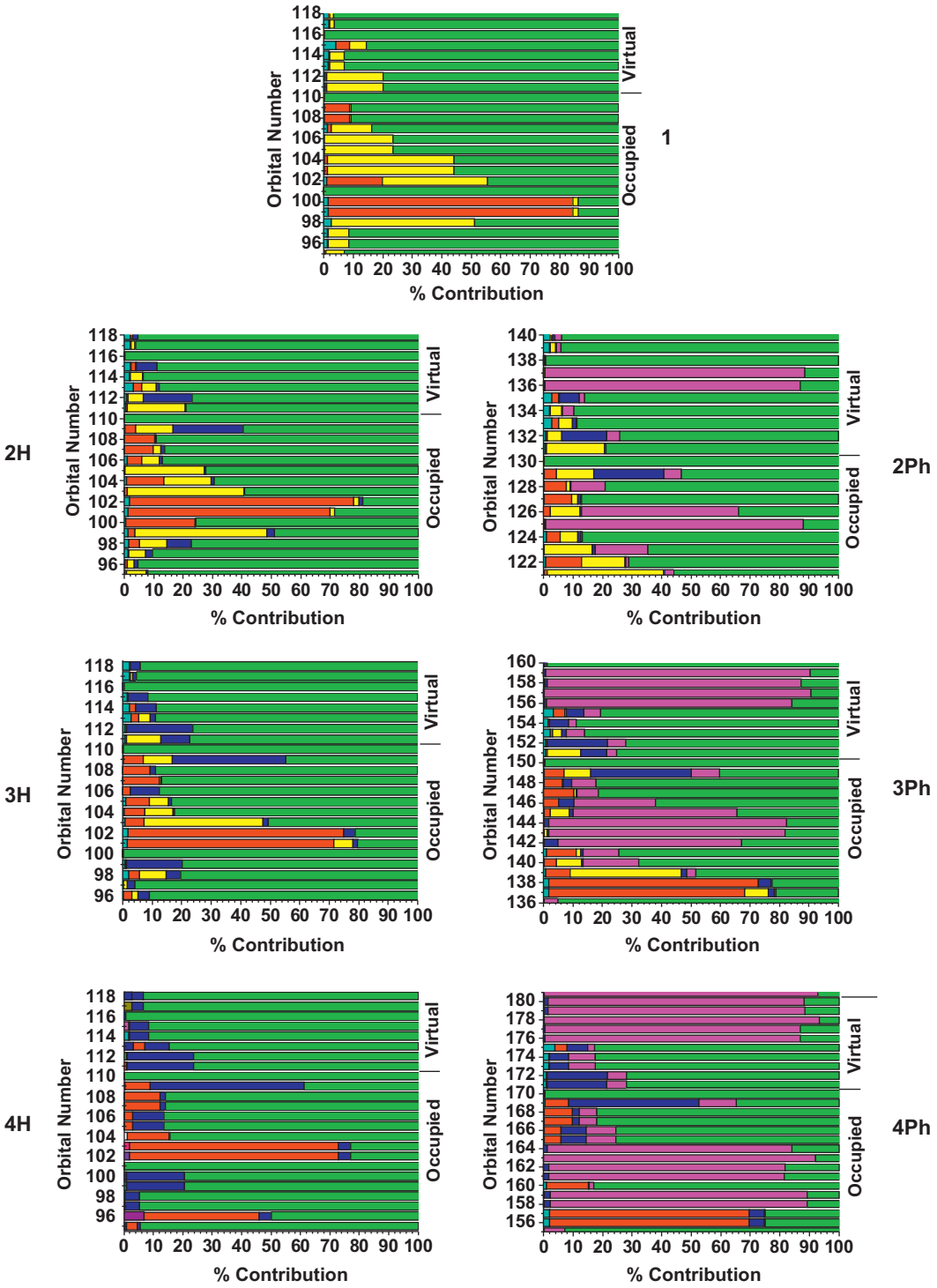

Fig. 3. Molecular orbital compositions for frontier orbitals in chloro-subphthalocyanine derivatives predicted at the DFT-BP86/6-311G(d) in dichloromethane solvent. Contributions from isoindole AOs are in green, *meso*-nitrogen atoms are in yellow, *meso*-carbons are in blue, chlorine atoms are in red, boron atom are in cyan and phenyl are in magenta.

subphthalocyanine reduces the molecular symmetry to Cs, lifts all degeneracy in MOs, and results in the increase of the HOMO–LUMO energy gap. The LUMO and LUMO+1 orbitals become separated by 0.15 eV. The HOMO in **2H** and **2Ph** has a″ symmetry and resembles the HOMO in **1** without any electron density localized at isoindole nitrogens and *meso*-atoms. Since the HOMO−1 and HOMO−2 pair in **1** has no electron density on *meso*-nitrogen atoms, while HOMO−3 has significant contribution from them, substitution of one *meso*-nitrogen atom in **1** by a CH fragment (**2H**) or CPh fragment (**2Ph**) results in significant destabilization of the former MO, which becomes a HOMO−1 in **2H** and **2Ph** (Fig. 2). Similarly, when two *meso*-nitrogen atoms are substituted by CH (**3H**) or CPh (**3Ph**) fragments, the HOMO−1 (which resembles HOMO−3 in **1**) becomes even more destabilized, while the change in energy of HOMO−2 and HOMO−3 (which resembles HOMO−1 and HOMO−2 pair in **1**) remains nearly constant. The HOMO–LUMO energy gap increases,

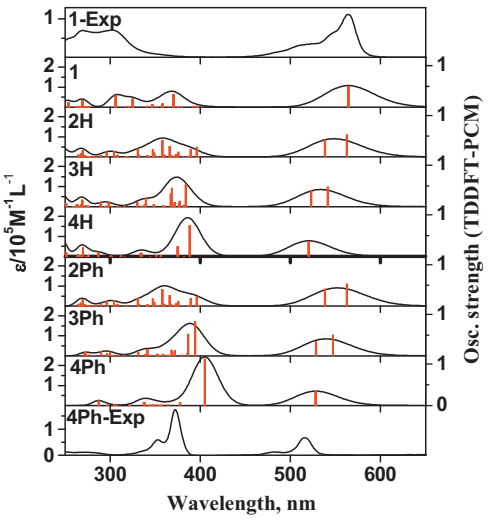

Fig. 4. Experimental and TDDFT predicted UV–vis spectra of the target complexes. Solid lines represent experimental or simulated data (FWHM = 1000 cm^{-1}), vertical red bar represents oscillator strength. (For interpretation of the references to color in this figure legend, the reader is referred to the web version of the article.)

while the LUMO and LUMO+1 energy separation remains close to that observed in **2H** and **2Ph**. Finally, the HOMO−1 in subporphyrins **4H** and **4Ph** is even more destabilized, while destabilization of the LUMO, LUMO+1, HOMO and the pair of the HOMO−2 and HOMO−3 MOs is small (Fig. 2).

Overall our DFT-PCM calculations revealed the following trends for the stepwise substitution of the *meso*-nitrogen atoms by CH or CPh fragments: (i) since the LUMO and LUMO+1 have a small contribution from the *meso*-atoms while HOMO has no contribution from *meso*-atoms, the LUMO destabilization is slightly larger relative to the destabilization of HOMO. This results in gradual increase of the HOMO–LUMO energy gap upon stepwise substitution of the *meso*-nitrogen atoms by CH or CPh groups; (ii) since the HOMO−1 (HOMO−3 in **1**) has a large contribution from the atoms located at *meso*-positions, it destabilizes much faster than the HOMO and LUMO. Such destabilization results in gradual decrease of the HOMO–HOMO−1 (HOMO−3 in **1**) gap upon substitution of the *meso*-nitrogen atoms by CH or CPh groups; (iii) contribution of the axial ligand σ-bond into HOMO−1 gradually increases with the increase of CH or CPh fragments at *meso*-positions. This could result in the stronger axial ligand effect in subporphyrins compared to subphthalocyanines. All of these general trends could directly affect the UV–vis spectroscopy of compounds **1**–**4**. Specifically, it is expected that the largest contribution to the Q-band region would originate from HOMO to LUMO/LUMO+1 electron excitations, while the most intense bands in B(Soret)-region should have predominant HOMO−1 (HOMO−3 in **1**) to LUMO/LUMO+1 character. If this hypothesis is correct, then based on DFT-PCM calculations, it can be expected that the Q-band should undergo a low-energy shift, while B(Soret)-band should undergo a higher-energy shifts upon gradual substitution of the *meso*-nitrogens in **1** by sp^2-hybrid carbon atoms.

In order to test this hypothesis, we have calculated vertical excitation energies in compounds **1**–**4** using TDDFT-PCM approach and compared the theoretical predictions with the experimentally available UV–vis spectra of subphthalocyanine **1** and subporphyrins **4H** and **4Ph**. The TDDFT predicted vertical excitation energies for targets studied are presented in Fig. 4, Figs. S8–S13 and Tables S8–S21 in Supporting Information. The calculated TDDFT-PCM UV–vis spectra for target compounds are shown in Fig. 4 along with the experimental spectra of **1** and **4Ph**. Although we tested TDDFT-PCM methods with and without solvent equilibration, the results are very close to each other and thus, we will only discuss the data obtained using solvent equilibration method below. In general, TDDFT-PCM data follow the expected trend from the electronic structure calculations, i.e. the Q-band region undergoes a higher-energy shift, while the B(Soret)-band region undergoes a lower-energy shift upon stepwise substitution of the *meso*-nitrogen atom by the CH or CPh fragments. When comparison with the experimental data is available (compounds **1**, **4H**, and **4Ph**), the calculated vertical excitation energies are in a good qualitative agreement with the experimental data.

In all complexes studied, the Q-band region indeed dominated by the first two excited states, which are almost entirely originating from HOMO → LUMO and HOMO → LUMO+1 transitions. Taking into consideration molecular symmetries and electronic structure compounds **1**–**4**, these excited states are doubly degenerate in the case of subphthalocyanine **1** and subporphyrins **4H** and **4Ph**, while the energy difference between Q_x (lower energy) and Q_y (higher energy) bands follows the degree of LUMO and LUMO+1 energy difference in **2H** and **2Ph** on one side and **3H** and **3Ph** on the other side. More importantly, the Q-band region undergoes a gradual higher-energy shift upon stepwise substitution of the *meso*-nitrogen atoms by the sp^2-hybrid carbon atoms in agreement with available experimental data (Fig. 4).

The B(Soret)-band region in C_{3v} symmetry compounds **1**, **4H**, and **4Ph** is dominated by the single electron excitations from a_1 MO (HOMO−3 in **1** and HOMO−1 in **4H** and **4Ph**) to doubly degenerate LUMO and LUMO+1. Again, TDDFT-PCM predicted red-energy shift in **4H** and **4Ph** compared to the B(Soret)-band position in **1** is in good agreement with the experimental data. The situation with the B(Soret)-band region in C_s symmetry compounds **2H**, **2Ph**, **3H**, and **3Ph** is more complex because single electron excitations originating from HOMO−1 (a′ symmetry) to LUMO and LUMO+1 undergo a strong configurational interaction with single electron excitations originating from HOMO−3 (a′ symmetry) to the LUMO and LUMO+1. As a result, two pairs of relatively strong bands are predicted in the B(Soret)-band region of these compounds. Nevertheless, as expected from electronic structure calculations, barycenter of the B(Soret)-band monotonically shifts to lower-energy region upon stepwise substitution of the *meso*-nitrogen atoms by the CH or CPh groups.

Overall, TDDFT-PCM calculations are in general agreement with the electronic structure and experimental data available on compounds **1**–**4**. Specifically, the Q-band region undergoes a higher-energy shift, while the B(Soret)-band region undergoes a lower-energy shift upon stepwise substitution of the *meso*-nitrogen atoms by CH or CPh fragments, which can be explained by monotonic increase of the HOMO–LUMO energy gap and gradual decrease of the HOMO–HOMO−1 (HOMO−3 in compound **1**) energy difference in compounds **1**–**4**.

4. Conclusions

Electronic structures, geometries, and vertical excitation energies of a chloro-substituted subphthalocyanine, tribenzodiazasubporphyrin, tribenzomonoazasubporphyrin, and tribenzosubporphyrin compounds **1**–**4** were calculated using DFT and TDDFT coupled with PCM approach. DFT-PCM and TDDFT-PCM calculations revealed the following general trends in studied compounds **1**–**4**: (i) although all compounds have bowl-shaped geometries, the depth of the bowl conformation decreases with increasing number of sp^2-hybrid atoms at the *meso*-positions of macrocycle; (ii) the HOMO–LUMO energy gap increases upon stepwise substitution of the *meso*-nitrogen atoms by CH or CPh groups; (iii) since HOMO−1 (HOMO−3 in **1**) has a large contribution from the atoms in *meso*-positions, it destabilizes much faster than the HOMO and

LUMO. Such destabilization results in a gradual decrease of the HOMO–HOMO−1 (HOMO−3 in **1**) gap upon substitution of the *meso*-nitrogen atoms by CH or CPh groups; (iv) contribution of the axial ligand σ-bond into HOMO−1 gradually increases with the increase of CH or CPh fragments at *meso*-positions; (v) the Q-band should undergo a gradual high-energy shift, while B-band should undergo low-energy shift upon stepwise substitution of the *meso*-nitrogen atoms in subphthalocyanine **1** toward tribenzosubporphyrins **4H** and **4Ph**. When comparison between theory and experiment is available, TDDFT-PCM calculations are in good qualitative agreement with experimental data.

Acknowledgements

Generous support from the NSF CHE-1110455 and Minnesota Supercomputing Institute to VN are greatly appreciated. Our work is partly supported by National Natural Science Foundation of China (Grant No. 20807037) and Zhejiang Provincial Natural Science Foundation of China (Grant No. LY12B07010).

Appendix A. Supplementary data

Supplementary data associated with this article can be found, in the online version, at http://dx.doi.org/10.1016/j.jmgm.2012.09.003.

References

[1] C.C. Leznoff, A.B.P. Lever (Eds.), Phthalocyanines: Properties and Applications, vols. 1–4, VCH Publishers, Ltd., Cambridge, 1989, 1993.
[2] C.G. Claessens, D. Gonzalez-Rodriguez, T. Torres, Subphthalocyanines: singular nonplanar aromatic compounds—synthesis, reactivity, and physical properties, Chemical Reviews 102 (2002) 835–853.
[3] A. Meller, A. Ossko, Phthalocyanine-like boron complexes. 15c-Halotriisoindolo[1,2,3-cd:1′,2′,3′-gh:1″,2″,3″-kl][2,3a,5,6a,8,9a,9b] hexaazaboraphenalenes, Monatshefte fur Chemie 103 (1972) 150–155.
[4] R.A. Kipp, J.A. Simon, M. Beggs, H.E. Ensly, R.H. Schmehl, Photophysical and photochemical investigation of a dodecafluorosubphthalocyanine derivative, Journal of Physical Chemistry A 102 (1998) 5659–5664.
[5] B. del Rey, U. Keller, T. Torres, G. Rojo, F. Agulló-López, F. Nonell, C. Martí, S. Brasselet, I. Ledoux, J. Zyss, Synthesis and nonlinear optical, photophysical and electrochemical properties of subphthalocyanines, Journal of the American Chemical Society 120 (1998) 12808–12817.
[6] K. Kasuga, T. Idehara, M. Handa, Y. Ueda, T. Fujiwara, K. Isa, Structure and some properties of (alkoxo)(subphthalocyaninato)boron(III), Bulletin of the Chemical Society of Japan 69 (1996) 2559–2563.
[7] P.V. Solntsev, K.L. Spurgin, J.R. Sabin, A.A. Heikal, V.N. Nemykin, Photoinduced charge transfer in short-distance ferrocenylsubphthalocyanine dyads, Inorganic Chemistry 51 (2012) 6537–6547.
[8] G.E. Morse, J.S. Castrucci, M.G. Helander, Z. Lu, T.P. Bender, Phthalimidoboronsubphthalocyanines. New derivatives of boronsubphthalocyanine with bipolar electrochemistry and functionality in OLEDs, ACS Applied Materials & Interfaces 3 (2011) 3538–3544.
[9] R.S. Iglesias, C.G. Claessens, T. Torres, M.A. Herranz, V.R. Ferro, J.M. Garcia de la Vega, Subphthalocyanine-fused dimers and trimers: synthetic, electrochemical and theoretical studies, Journal of Organic Chemistry 72 (2007) 2967–2977.
[10] A. Sastre, T. Torres, M.A. Díaz-García, F. Agulló-López, C. Dhenaut, S. Brasselet, I. Ledoux, J. Zyss, Subphthalocyanines novel targets for remarkable second-order optical nonlinearities, Journal of the American Chemical Society 118 (1996) 2746–2747.
[11] M. Geyer, F. Plenzig, J. Rauschnabel, M. Hanack, B. Del Rey, A. Sastre, T. Torres, Subphthalocyanines: preparation, reactivity and physical properties, Synthesis 9 (1996) 1139–1151.
[12] M.A. Diaz-Garcia, M. Agullo-Lopez, A. Sastre, T. Torres, W.E. Torruellas, G.I. Stegeman, Third harmonic generation spectroscopy of boron subphthalocyanine, Journal of Physical Chemistry 99 (1995) 14988–14991.
[13] I. Ledoux, J. Zyss, From one-to two-dimensional complexes for quadratic nonlinear optics: the influence of ligand and complexing metal atoms, Pure and Applied Optics 5 (1996) 603–612.
[14] H. Gommans, T. Aernouts, B. Verreet, P. Heremans, A. Medina, C.G. Claessens, T. Torres, Perfluorinated subphthalocyanine as a new acceptor material in a small-molecule bilayer organic solar cell, Advanced Functional Materials 19 (2009) 3435–3439.
[15] C.E. Mauldin, C. Piliego, D. Poulsen, D.A. Unruh, C. Woo, B. Ma, J.L. Mynar, J.M.J. Fréchet, Axial thiophene-boron(subphthalocyanine) dyads and their application in organic photovoltaics, ACS Applied Materials & Interfaces 2 (2010) 2833–2838.
[16] J.Y. Kim, S. Noh, Y.M. Nam, J.Y. Kim, J. Roh, M. Park, J.J. Amsden, D.Y. Yoon, C. Lee, H.J. Won, Effect of nanoscale SubPc interfacial layer on the performance of inverted polymer solar cells based on P3HT/PC_{71}BM, ACS Applied Materials & Interfaces 3 (2011) 4279–4285.
[17] G.E. Morse, M.G. Helander, J.F. Maka, Z.H. Lu, T.P. Bender, Fluorinated phenoxy boron subphthalocyanines in organic light-emitting diodes, ACS Applied Materials & Interfaces 2 (2010) 1934–1944.
[18] D.D. Diaz, H.J. Bolink, L. Cappelli, C.G. Claessens, E. Coronado, T. Torres, Subphthalocyanines as narrow band red-light emitting materials, Tetrahedron Letters 48 (2007) 4657–4660.
[19] D. Dini, S. Vagin, M. Hanack, V. Amendola, M. Meneghetti, Nonlinear optical effects related to saturable and reverse saturable absorption by subphthalocyanines at 532 nm, Chemical Communications (2005) 3796–3798.
[20] A. Sastre, B. Del Rey, T. Torres, Synthesis of novel unsymmetrically substituted push–pull phthalocyanines, Journal of Organic Chemistry 61 (1996) 8591–8597.
[21] G. Martin, G. Rojo, F. Agullo-Lopez, V.R. Ferro, J.M. Garcia de la Vega, M.V. Martinez-Diaz, T. Torres, I. Ledoux, J. Zyss, Subphthalocyanines and subnaphthalocanines nonlinear quasi-planar octapolar systems with permanent polarity, Journal of Physical Chemistry B 106 (2002) 13139–13145.
[22] C.G. Claessens, D. Gonzalez-Rodriguez, T. Torres, Subphthalocyanines: singular nonplanar aromatic compounds—synthesis, reactivity and physical properties, Chemical Reviews 102 (2002) 835–853.
[23] H. Xu, X.-J. Jiang, E.Y.M. Chan, W.-P. Fong, D.K.P. Ng, Synthesis, photophysical properties and in vitro photodynamic activity of axially substituted subphthalocyanines, Organic & Biomolecular Chemistry 5 (2007) 3987–3992.
[24] N. Rubio, A. Jim_enez-Banzo, T. Torres, S. Nonell, Spectral and kinetic properties of the radical ions of chloroboron(III) subnaphthalocyanine, Journal of Photochemistry and Photobiology A 185 (2007) 214–219.
[25] J. Liu, H. Yeung, W. Xu, X. Li, D.K.P. Ng, Highly efficient energy transfer in subphthalocyanine–BODIPY conjugates, Organic Letters 10 (2008) 5421–5424.
[26] F. Camerel, G. Ulrich, P. Retailleau, R. Ziessel, Ethynyl-boron subphthalocyanines displaying efficient cascade energy transfer and large stokes shifts, Angewandte Chemie International Edition 47 (2008) 8876–8880.
[27] A. Medina, C.G. Claessens, G.M. Aminur Rahman, A.M. Lamsabhi, O. Mó, M. Yáñez, D.M. Guldi, T. Torres, Accelerating charge transfer in a triphenylamine–subphthalocyanine donor–acceptor system, Chemical Communications (2008) 1759–1761.
[28] D. González-Rodríguez, T. Torres, D.M. Guldi, J. Rivera, M.Á. Herranz, L. Echegoyen, Subphthalocyanines tuneable molecular scaffolds for intramolecular electron and energy transfer processes, Journal of the American Chemical Society 126 (2004) 6301–6313.
[29] B.A. Kamino, G.E. Morse, T.P. Bender, Effect of triarylamine structure on the photoinduced electron transfer to boron subphthalocyanine, Journal of Physical Chemistry C 115 (2011) 20716–20723.
[30] Y. Inokuma, J.H. Kwon, T.K. Ahn, M. Yoo, D. Kim, A. Osuka, Tribenzosubporphines: synthesis and characterization, Angewandte Chemie International Edition 45 (2006) 961–964.
[31] E.A. Makarova, S. Shimizu, A. Matsuda, E.A. Luk'yanets, N. Kobayashi, meso-Aryl tribenzosubporphyrin—a totally substituted subporphyrin species, Chemical Communications (2008) 2109–2111.
[32] M.J. Frisch, G.W. Trucks, H.B. Schlegel, G.E. Scuseria, M.A. Robb, J.R. Cheeseman, G. Scalmani, V. Barone, B. Mennucci, G.A. Petersson, H. Nakatsuji, M. Caricato, X. Li, H.P. Hratchian, A.F. Izmaylov, J. Bloino, G. Zheng, J.L. Sonnenberg, M. Hada, M. Ehara, K. Toyota, R. Fukuda, J. Hasegawa, M. Ishida, T. Nakajima, Y. Honda, O. Kitao, H. Nakai, T. Vreven, J.A. Montgomery Jr., J.E. Peralta, F. Ogliaro, M. Bearpark, J.J. Heyd, E. Brothers, K.N. Kudin, V.N. Staroverov, R. Kobayashi, J. Normand, K. Raghavachari, A. Rendell, J.C. Burant, S.S. Iyengar, J. Tomasi, M. Cossi, N. Rega, J.M. Millam, M. Klene, J.E. Knox, J.B. Cross, V. Bakken, C. Adamo, J. Jaramillo, R. Gomperts, R.E. Stratmann, O. Yazyev, A.J. Austin, R. Cammi, C. Pomelli, J.W. Ochterski, R.L. Martin, K. Morokuma, V.G. Zakrzewski, G.A. Voth, P. Salvador, J.J. Dannenberg, S. Dapprich, A.D. Daniels, O. Farkas, J.B. Foresman, J.V. Ortiz, J. Cioslowski, D.J. Fox, Gaussian 09, Gaussian, Inc., Wallingford, CT, 2009.
[33] M. Caricato, B. Mennucci, J. Tomasi, F. Ingrosso, R. Cammi, S. Corni, G. Scalmani, Formation and relaxation of excited states in solution: a new time dependent polarizable continuum model based on time dependent density functional theory, Journal of Chemical Physics 124 (2006) 124520–124532.
[34] A.D. Becke, Density-functional exchange-energy approximation with correct asymptotic behavior, Physical Review A 38 (1988) 3098–3100.
[35] J.P. Perdew, Density functional approximation for the correlation energy of the inhomogeneous electron gas, Physical Review B 33 (1986) 8822–8824.
[36] A.D. McLean, G.S. Chandler, Contracted Gaussian basis sets for molecular calculations. I. Second row atoms, $Z = 11–18$, Journal of Chemical Physics 72 (1980) 5639–5648.
[37] S. Sripothongnak, C.J. Ziegler, M.R. Dahlby, V.N. Nemykin, Controllable and reversible inversion of the electronic structure in nickel N-confused porphyrin: a case when MCD matters, Inorganic Chemistry 50 (2011) 6902–6909.
[38] V.N. Nemykin, R.G. Hadt, R.V. Belosludov, H. Mizuseki, Y. Kawazoe, Influence of molecular geometry, exchange-correlation functional, and solvent effects in the modeling of vertical excitation energies in phthalocyanines using time-dependent density functional theory (TDDFT) and polarized continuum model TDDFT methods: can modern computational chemistry methods

explain experimental controversies? Journal of Physical Chemistry A 111 (2007) 12901–12913.
[39] G.A. Peralta, M. Seth, T. Ziegler, Magnetic circular dichroism of porphyrins containing M) Ca, Ni, and Zn. A computational study based on time-dependent density functional theory, Inorganic Chemistry 46 (2007) 9111–9125.
[40] A.L. Tenderholt, QMForge: A Program to Analyze Quantum Chemistry Calculations, Version 2.1, http://qmforge.sourceforge.net
[41] H. Kietaibl, Crystal and molecular structure of a new phthalocyanine-like boron complex, Monatshefte fur Chemie 105 (1974) 405–418.
[42] V.R. Ferro, J.M. García de la Vega, R.H. González-Jonte, L.A. Poveda, Theoretical study of subphthalocyanine and its nitro- and tertbutyl-derivatives, Journal of Molecular Structure (Theochem) 537 (2001) 223–234.
[43] S. Yamauchi, A. Takahashi, Y. Iwasaki, M. Unno, Y. Ohba, J. Higuchi, A. Blank, H. Levanon, The lowest photoexcited triplet state of subphthalocyanine in solid and fluid environments. Time-resolved electron paramagnetic resonance studies, Journal of Physical Chemistry A 107 (2003) 1478–1485.
[44] Y. Yang, Metal–ligand coordination in subphthalocyanines and phthalocyanines: DFT, AIM and ELF analyses, Polyhedron 33 (2012) 310–318.